

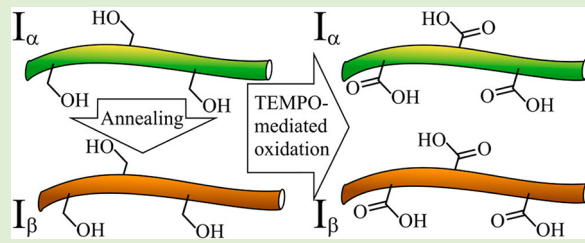
Susceptibility of I_{α} - and I_{β} -Dominated Cellulose to TEMPO-Mediated Oxidation

Daniel O. Carlsson,* Jonas Lindh, Maria Strømme, and Albert Mihranyan*

Nanotechnology and Functional Materials, Department of Engineering Sciences, Uppsala University, Box 534, 751 21 Uppsala, Sweden

Supporting Information

ABSTRACT: The susceptibility of I_{α} - and I_{β} -dominated cellulose to TEMPO-mediated oxidation was studied in this work since the cellulose I_{α} -allomorph is generally considered to be thermodynamically less stable and therefore more reactive than the cellulose I_{β} -allomorph. Highly crystalline *Cladophora* nanocellulose, which is dominated by the I_{α} -allomorph, was oxidized to various degrees with TEMPO oxidant via bulk electrolysis in the absence of co-oxidants. Further, the *Cladophora* nanocellulose was thermally annealed in glycerol to produce its I_{β} -dominated form and then oxidized. The produced materials were subsequently studied using FTIR, CP/MAS ^{13}C NMR, XRD, and SEM. The solid-state analyses confirmed that the annealed *Cladophora* cellulose was successfully transformed from an I_{α} to an I_{β} -dominated form. The results of the analyses of pristine and annealed TEMPO-oxidized samples suggest that I_{α} - and I_{β} -dominated cellulose do not differ in susceptibility to TEMPO-oxidation. This work hence suggests that cellulose from different sources are not expected to differ in susceptibility to the oxidation due to differences in allomorph composition.



INTRODUCTION

Cellulosic nanomaterials, such as cellulose nanocrystals (CNC) and cellulose nanofibers (CNF), are some of the most investigated nanomaterials today.¹ Their large-scale production has been facilitated by the development of new methods of cellulose defibrillation into nanoscale units at reduced energy consumption. Among mechanochemical methods of nanocellulose production TEMPO-mediated oxidation has become widespread due to its ease and efficiency. A comprehensive review on the methodology of TEMPO-mediated oxidation of carbohydrates can be found in ref 2. Briefly, the method relies on oxidation of primary C6 hydroxyls to carboxylates (and partially aldehydes) on the surface of cellulose fibrils. The generated net negative charge on the surface of cellulose fibrils produces electrostatic repulsion between adjacent units and thereby significantly facilitates the process of cellulose defibrillation. Traditionally, TEMPO-mediated oxidation of cellulose is conducted at pH 10 in the presence of NaBr and NaClO, which are used as regenerators for the TEMPO oxidant. The oxidation can also be conducted at pH 6.8 using NaClO and NaClO₂ as regenerating agents.³ Alternatively, the TEMPO-mediated oxidation of cellulose can be conducted electrochemically via bulk electrolysis, thereby eliminating the use of halogenated co-oxidants to regenerate the TEMPO oxidant.^{4–6}

It is often stated in the literature that TEMPO-mediated oxidation is a regioselective surface-limited method of cellulose oxidation because only primary C6 hydroxyls located on the surface of cellulose fibrils are reacted.² However, the fundamental understanding of the susceptibility of various

cellulose types to TEMPO-mediated oxidation is still limited. Isogai and coauthors have studied the susceptibility of cellulose samples from varying sources to TEMPO-oxidation and found that cellulose samples featuring large crystallite size, such as algae and bacterial cellulose, tend to be less susceptible to TEMPO-mediated oxidation than those featuring small crystallite size.⁷ In particular, the maximum total carboxylate/aldehyde content of softwood cellulose (average crystallite size 3.8 nm), cotton (average crystallite size 5.4 nm), bacterial cellulose (average crystallite size 5.8 nm) and cellulose obtained from *Cladophora* algae (average crystallite size 13.1 nm) was inversely (albeit not linearly) related to the crystallite size, namely, 1.72 mmol/g for softwood, 1.36 mmol/g for cotton, 1.15 mmol/g for bacterial cellulose, and 0.52 mmol/g for *Cladophora* cellulose. These results highlighted the importance of the available fibril surface area for TEMPO-mediated oxidation, as related to the crystallite size. However, in spite of a number of useful insights, the study by Isogai and coauthors was inconclusive whether cellulose materials featuring different ratio of cellulose I allomorphs, namely, algae-bacterial versus cotton-ramie types, exhibit different susceptibility to TEMPO-mediated oxidation.

Native cellulose (or cellulose I) consists of two allomorphs, that is, cellulose I_{α} , also known as algae-bacterial type, and cellulose I_{β} , also known as cotton-ramie type.⁸ The allomorph I_{α} has a triclinic cell unit of the following dimensions, $a = 0.674$

Received: February 27, 2015

Revised: March 31, 2015

Published: April 1, 2015

nm, $b = 0.593$ nm, $c = 1.036$ nm, $\alpha = 117^\circ$, $\beta = 114^\circ$, and $\gamma = 81^\circ$, whereas cellulose I_β is monoclinic and features a cell unit of the following dimensions: $a = 0.801$ nm, $b = 0.817$ nm, $c = 1.036$ nm, $\alpha = \beta = 90^\circ$, and $\gamma = 97.3^\circ$.⁹ Usually, both allomorphs coexist in varying proportions in plants and other cellulose-producing organisms. It has been observed that higher order organisms, producing I_β -dominated cellulose, typically feature rosette-type terminal synthase complexes (TCs), while primitive organisms, producing I_α -dominated cellulose, lack rosette TCs and instead feature linear or large rectangular synthase complexes.¹⁰ Although, this rule is generally valid for most organisms, exceptions also exist. Therefore, the exact reasons for formation of different allomorphs and more importantly their coexistence in the same organism are still unclear. It should be mentioned that essentially pure (>90%) cellulose I_α could be obtained from *Glaucocystis* sp. algae,¹¹ whereas essentially pure cellulose I_β can be extracted from *Halocyrtia* sp. tunicates.¹² According to one of the hypotheses, the formation of cellulose I_α is favored by bending and mechanical stresses experienced during cellulose synthesis, since *Glaucocystis* algae are spherical.¹¹ The latter hypothesis found some support by computational modeling, which suggests that bending of cellulose chains prior to formation of cellulose fibrils might result in a different cell unit than that otherwise produced. In particular, a bending angle of 39° could be sufficient for transition from one allomorph to the other.¹³ The transition between the allomorphs can also be induced in vitro by physical-chemical means. The most common way to induce transition from the cellulose I_α -dominated form to the cellulose I_β -dominated one is through thermal annealing, which can be achieved in (i) water,^{14–16} (ii) organic solvents,¹⁷ or (iii) inert gas.¹⁸ Alternatively, the transition can be achieved using ultrasonic radiation¹⁹ or by solid-state saponification from cellulose triacetate.²⁰ Furthermore, transition of cellulose I_α to cellulose I_β was reported in *Acetobacter xylinum* bacterial cultures enriched with hemicellulose precursors,^{19,21,22} for example, xyloglucan and glucomannan, in spite of the fact that bacteria lack rosette-type TCs.

It is conceived that cellulose I_α is thermodynamically less stable and therefore more reactive than cellulose I_β .^{14–16} The experimental evidence of higher reactivity is manifold: (i) cellulose I_α is more susceptible to acetylation reactions than cellulose I_β ,^{23,24} (ii) cellulose I_α is more prone to acidic hydrolysis than cellulose I_β ,^{10,25} and (iii) cellulose I_α exhibits higher propensity to enzymatic degradation by *Trichoderma* sp. cellulases than cellulose I_β , as indicated by larger weight loss and gradual transition from one allomorph to the other upon extended enzymatic treatment.^{9,26} The differences in the reactivity of cellulose I_α and I_β have led to another controversy related to the coexistence of these allomorphs, namely their exact location within elementary fibrils. It was first postulated that the reactive cellulose I_α is preferentially located at the surface of fibrils whereas cellulose I_β is distributed mainly inside the core.²⁵ The alternative model disputed the core–shell model of allomorph distribution and suggested that they were distributed throughout the entire fibril, alternating either longitudinally or laterally.²⁷

Considering the widespread use of TEMPO-mediated oxidation for production of cellulosic nanomaterials, a better fundamental understanding of the process is required on the structural level, and several questions need to be addressed. The foremost question is whether cellulose I_α is more susceptible to carboxylation via TEMPO-mediated oxidation

than cellulose I_β in analogy with the acetylation reaction and enzymatic hydrolysis.

In an attempt to address the issue of susceptibility to TEMPO-oxidation of I_α - and I_β -dominated celluloses, electrochemically controlled co-oxidant-free TEMPO-mediated oxidation, previously described by our group,⁶ of *Cladophora* sp. cellulose was employed, followed by comprehensive structural characterization. The structural characterization of the solid-state properties of carboxylated *Cladophora* nanocellulose as a function of oxidation charge was performed using CP/MAS ^{13}C NMR, XRD, and FTIR. The use of *Cladophora* cellulose was motivated by its high cellulose I_α content and exceptionally high crystallinity,²⁸ which minimizes the reactivity contribution of amorphous cellulose. Further, co-oxidant-free TEMPO-mediated bulk electrolysis oxidation was deemed particularly useful, as it eliminates the interference of halogenated co-oxidants during the oxidation. As a reference, we induced the transition of *Cladophora* nanocellulose to its I_β -dominated form by thermal annealing in glycerol and compared its susceptibility to TEMPO-mediated oxidation in the pristine form. The aim of the present work is thus to explore if there is a difference in susceptibility to TEMPO-mediated oxidation between I_α - and I_β -dominated cellulose to gain further fundamental knowledge related to the reactivity of cellulose from different sources.

EXPERIMENTAL SECTION

Materials. *Cladophora* sp. algae nanocellulose was obtained as a spray-dried powder (hemicellulose content < 1%) from FMC Biopolymers (U.S.A.). All chemicals were of reagent or analytical grade and were used as received from commercial suppliers. Deionized water was used throughout all experiments.

Methods. Annealing Treatment. The annealing procedure was based on an earlier report, where successful transformation of I_α to I_β in glycerol was reported, with some modifications.²⁹ *Cladophora* nanocellulose, 10 g, was added to ~250 mL of glycerol. The mixture was heated to 290 °C and held at that temperature for the duration of the annealing treatment (1 h). The reaction vessel was fitted with a water-cooled spiral cooler. The mixture was subsequently cooled and thoroughly washed through centrifugation (4700g) with water, followed by ethanol until the liquid phase was colorless, and finally with water again. The product was subsequently freeze-dried.

TEMPO-Mediated Oxidation in a Bulk Electrolysis Setup. The oxidation of pristine *Cladophora* nanocellulose was reported in our earlier work and the same procedure was employed in the current work with annealed *Cladophora*.⁶ Briefly, 150 mg of TEMPO and 750 mg of *Cladophora* nanocellulose was added to 175 mL of 0.1 M carbonate buffer (pH 10.3) in the main compartment of the electrochemical cell, along with a graphite working electrode (~12 cm²). The counter electrode (coiled Pt-wire, ~3 cm²) and reference electrode (3 M NaCl Ag/AgCl) were placed in separate compartments (sintered glass filters, 4–8 μm pores). The potential was controlled at 0.7 V versus Ag/AgCl by an Autolab potentiostat (EcoChemie, The Netherlands). The electrolysis was carried out under vigorous stirring and was stopped when 285 °C had been reached, corresponding to the charge needed in order to fully oxidize the surface of pristine *Cladophora* nanocellulose.⁶ Ethanol was immediately added for quenching and the product was washed by centrifugation (4700g) with ethanol and then dialyzed in water for 3 days. The product was collected in 0.01 M HCl through centrifugation (4700g), and the solvent was then exchanged to ethanol, followed by ether, and finally dried from ether.

Conductometric Titration. The carboxylic acid content was determined through conductometric titrations. Approximately 100 mg of sample was dispersed in 60 mL of 0.010 M NaCl (aq) through high-energy ultrasonication (VibraCell, U.S.A.), and the pH was adjusted to <3 with concentrated HCl. The dispersion was equilibrated at 25 °C with nitrogen purging for 30 min prior to titrations and the

titrations were carried out under nitrogen atmosphere with addition of 0.020 mL of 0.050 M NaOH (aq) every 30 s until pH \sim 11. Line fitting of the linear regions (corresponding to strong acid and base) and of the plateau region (corresponding to weak acid, i.e., carboxylic acid) of the conductivity versus titration volume curves were made and the carboxylic acid content was calculated from the intercepts of the fitted lines. Each sample was analyzed three times. Two-sided *t* test (95% confidence interval) was used to statistically compare the carboxylic acid contents in the samples, as described by Miller and Miller.³⁰

Fourier Transform Infrared Spectroscopy. KBr pellets (1 wt % sample) were prepared and spectra were collected on a Bruker Tensor 27 (Germany) FTIR instrument at 4 cm⁻¹ resolution. To collect the spectra, 100 scans were averaged and a rubberband background was subtracted from all spectra using the instrument software (Opus 7.0, Bruker, Germany). The spectra were normalized with respect to the absorption at 2897 cm⁻¹, corresponding to a C–H stretching vibration.³¹

The I_α fraction, f_α , of the samples was estimated as previously described by Imai and Sugiyama,³² that is, by applying eq 1;

$$f_\alpha = \frac{A_{750}}{A_{750} + kA_{710}} \times 100\% \quad (1)$$

where A_{750} and A_{710} are the areas of the 750 and 710 cm⁻¹ peaks that are specific I_α and I_β vibrations, respectively, and k is the ratio of the absorption coefficients between the peaks ($k = \epsilon_{750}/\epsilon_{710}$), taken to be $k = 0.16$ as earlier reported.³² A_{750} and A_{710} were obtained by subtracting a local linear background between approximately 770 and 690 cm⁻¹ followed by integration of the peaks using Origin 9.1 (OriginLab Corp., U.S.A.).

Solid-State CP/MAS ¹³C NMR. All NMR experiments were performed on a Varian Inova-600 operating at 14.7 T and equipped with a 3.2 mm solid-state probe. Measurements were conducted at 301 K with a MAS spinning rate of 15 kHz. The CP/MAS ¹³C NMR spectra were recorded using a cross-polarization pulse sequence followed by proton decoupling during acquisition. Acquisition parameters included a 2.9 μ s ¹H 90°-pulse, 1200 μ s contact time, 25 ms acquisition time, and 54 s recycle delay to allow for complete thermal equilibrium. A crystallinity index (CrI(NMR)) was calculated according to a previously published method,³³ by integrating the signals at 86–92 (A) and 80–86 ppm (B) and applying eq 2.

$$\text{CrI}(\text{NMR}) = \frac{A}{A + B} \times 100\% \quad (2)$$

X-ray Diffraction. An X-ray diffractometer (D5000, Siemens/Bruker, Germany) with Bragg–Brentano geometry (Cu K α radiation; $\lambda = 1.54$ Å) was used. $\Delta 2\theta$ was 0.01°/step and the step time was 1 or 2 s. A XRD crystallinity index (CrI(XRD)) was calculated from the raw data according to eq 3;³⁴

$$\text{CrI}(\text{XRD}) = \frac{I_{22} - I_{18}}{I_{22}} \times 100\% \quad (3)$$

where I_{22} is the maximum intensity at approximately $2\theta = 22.5^\circ$ and I_{18} is the intensity at $2\theta = 18^\circ$.

A spline background was subtracted and a pseudo-Voigt function was fitted to the data using Origin 9.1 (OriginLab corp., U.S.A.). d -Spacings between the crystal planes, d , and the crystallite sizes, L , were derived from the fitted curves according to Bragg's law (eq 4) and the Scherrer equation (eq 5), respectively.³⁵

$$d = \lambda 2 \sin \theta \quad (4)$$

$$L = 0.9\lambda H \cos \theta \quad (5)$$

where $\lambda = 1.54$ Å, H is the full width at half-maximum (fwhm), and θ is the Bragg angle. Two diffractograms were collected for each sample.

Scanning Electron Microscopy. Scanning electron micrographs were recorded on a LEO1550 field emission SEM instrument (Zeiss, Germany). Samples were mounted on aluminum stubs with double-

sided adhesive carbon tape and sputtered with Au/Pd to reduce charging effects.

RESULTS AND DISCUSSION

Carboxylic Acid Content. In our earlier work,⁶ we demonstrated that pristine *Cladophora* nanocellulose can be completely surface-oxidized through co-oxidant-free TEMPO-mediated oxidation in an electrochemical setup. The degree of oxidation could be controlled by controlling the oxidation time or, more accurately, by controlling the charge that passed through the system. In that work we characterized the material in terms of, for example, carboxylic acid content. In the present work we further characterize those materials and compare them to annealed samples. For clarity, the oxidation time, passed charge, and the resulting carboxylic acid content are therefore reproduced in Table 1. A pristine *Cladophora* nanocellulose

Table 1. Oxidation Time, Passed Charge, Carboxylic Acid Content, and Degree of Oxidation for I_α - or I_β -Dominanted *Cladophora* Nanocellulose Samples^a

sample name	description	oxidation time (h/min)	charge passed ^b (C)	carboxylic acid content ^c ($\mu\text{mol/g}$)	degree of oxidation ^d (%)
$\alpha_0.6$	pristine	0:00	0	37 ± 2	0.6
$\alpha_1.3$	oxidized	0:30	36 ± 1	79 ± 7	1.3
$\alpha_2.3$	oxidized	1:00	69 ± 3	143 ± 13	2.3
$\alpha_4.9$	oxidized	2:00	141 ± 6	301 ± 9	4.9
$\alpha_7.5$	oxidized	3:00	208 ± 5	461 ± 10	7.5
$\alpha_9.7$	oxidized	4:00	285 ± 7	591 ± 10	9.7
$\beta_0.8$	annealed	0:00	0	47 ± 9	0.8
$\beta_9.3$	annealed and oxidized	4:45	285	569 ± 20	9.3

^aData for samples $\alpha_0.6$ through $\alpha_9.7$ are reproduced from ref 6.

^bValues represent the mean \pm standard deviation ($n = 3$) for samples $\alpha_1.3$ through $\alpha_9.7$, $n = 1$ for $\beta_9.3$. ^cValues represent the mean \pm standard deviation ($n = 3$). ^dBased on the carboxylic acid mean value.

sample, that is, a sample not subjected to TEMPO-mediated oxidation (denoted $\alpha_0.6$), contained 0.037 ± 0.002 mmol/g of carboxylic acids, which corresponds to a degree of oxidation of 0.6% with respect to C6 carboxylic acid. A maximum degree of oxidation of 9.7%, corresponding to 0.591 ± 0.010 mmol/g of carboxylic acids, was achieved after a total charge of 285 C had been applied. This sample is consequently denoted $\alpha_9.7$.

In the present work, pristine *Cladophora* nanocellulose was annealed in glycerol at 290 °C for 1 h, in order to produce I_β -dominated *Cladophora* nanocellulose, using a procedure similar to a previously described method.³² The annealing was successful, that is, the crystallites were transformed from being I_α -dominated to being I_β -dominated, as will be evidenced in later sections. Following annealing, the carboxylic acid content was 0.047 ± 0.009 mmol/g (sample denoted $\beta_0.8$), which was not significantly different from $\alpha_0.6$ (95% confidence interval). Annealed *Cladophora* nanocellulose subjected to 285 °C of TEMPO-mediated oxidation (sample $\beta_9.3$) contained 0.569 ± 0.020 mmol/g of carboxylic acids. There was no statistically significant difference between the carboxylic acid contents of $\alpha_9.7$ and $\beta_9.3$ (95% confidence interval).

Structural Characterization. Pristine and annealed *Cladophora* cellulose samples, before and after oxidation, were further characterized with FTIR, solid state CP/MAS ¹³C

NMR, XRD, and SEM in order to evaluate structural characteristics. Samples α _1.3 through α _7.5 are omitted in the figures for brevity, but the corresponding data can be found in the Supporting Information (Figures S1–3).

The FTIR spectra for the 4000–400 cm^{-1} region are presented in Figure 1A. As seen, the intensity and peak area of

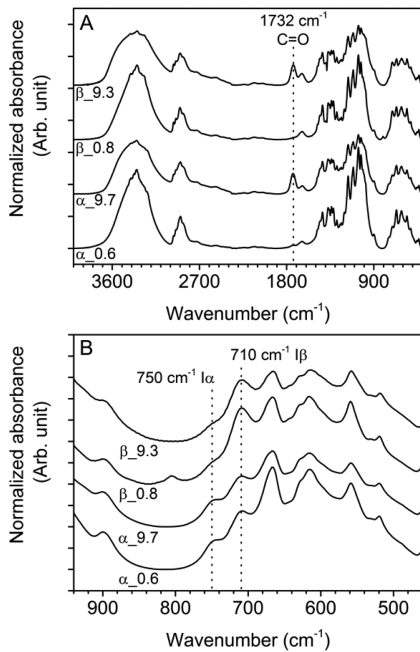


Figure 1. FTIR spectra of pristine and annealed *Cladophora* nanocellulose samples α _0.6, α _9.7, β _0.8, and β _9.3: (A) 4000–400 cm^{-1} and (B) 940–460 cm^{-1} region. Corresponding spectra for all samples, including samples α _1.3 through α _7.5, are shown in Supporting Information, Figure S1.

the carbonyl peak at 1732 cm^{-1} is similar for α _9.7 and β _9.3 samples, corroborating that the carboxylic acid content indeed is very similar in the two samples. Furthermore, the lack of the carbonyl peak in α _0.6 and β _0.8 confirms their low carboxylic acid content.

FTIR spectroscopy has been routinely used to assess the relative ratio between I_α - and I_β -allomorphs. In particular, the absorbance bands at 3240 and 750 cm^{-1} as well as 3270 and 710 cm^{-1} have been assigned to cellulose I_α and cellulose I_β , respectively.³² Spectra, zoomed in on the region 940–460 cm^{-1} for visualization of the relative cellulose I_α - or I_β contents, are shown in Figure 1B.

The fraction of cellulose I_α in the samples was estimated according to eq 1 based on the relative peak areas of the 750 cm^{-1} and the 710 cm^{-1} bands in the FTIR spectra, and the results are summarized in Table 2. The cellulose I_α content decreased from 74% to 15% following the thermal annealing, while the fraction was virtually unaffected by TEMPO-mediated oxidation.

CP/MAS ^{13}C NMR was used to obtain the crystallinity index (CrI(NMR)) and qualitatively assess I_α - and I_β -allomorphs in the studied samples. The CP/MAS ^{13}C NMR spectra for the C1–C6 region for α _0.6, α _9.7, and β _0.8 through β _9.3 are presented in Figure 2, and Table 2 summarizes the crystallinity index values obtained from NMR. The full range of obtained spectra for all studied samples is presented in Supporting Information, Figure S2. It is seen in Figure 2 that thermal

Table 2. Summary of the Fraction of Cellulose I_α Estimated from FTIR as Well as Crystallinity Indices Estimated from CP/MAS ^{13}C NMR and XRD

sample name	f_α (FTIR; %); $n = 1$	CrI(NMR) (%); $n = 1$	CrI(XRD) (%); ^a $n = 2$
α _0.6	74	83	93.4 \pm 0.7
α _1.3	74	81	93.0 \pm 2.0
α _2.3	76	78	92.4 \pm 1.2
α _4.9	76	81	92.3 \pm 1.4
α _7.5	77	75	92.7 \pm 1.0
α _9.7	77	77	93.8 \pm 1.2
β _0.8	15	83	91.7 \pm 0.8
β _9.3	16	85	89.6 \pm 0.6

^aValues represent the mean \pm absolute deviation ($n = 2$).

annealing resulted in successful transition from the I_α -dominated structure to the I_β -dominated one. The latter is specifically illustrated by comparison of the signals for the C1-region between 105 and 108 ppm in Figure 3. It is seen in Figure 3 that the proportion of the I_α -fraction was substantially reduced during the thermal annealing as manifested by decreased intensity of the I_α -peak, whereas the intensity of the I_β -peaks increased. No substantial differences were observed between samples of varying degree of oxidation of the I_α - and I_β -dominated specimens, respectively. These trends are in accordance with the estimated I_α -fraction (f_α) values presented above. As is further seen from Table 2, the crystallinity index values obtained from NMR spectroscopy did not suggest major changes in the degree of crystallinity following neither annealing nor TEMPO-mediated oxidation.

XRD was used to further verify the transitions between allomorphs of cellulose. The triclinic and monoclinic unit cells for each allomorph feature characteristic peaks in XRD, and shifts in the relative position of the peaks can be used to detect transition from one allomorph to the other. The diffractograms for α _0.6, α _9.7, β _0.8, and β _9.3 are shown in Figure 4, and Table 2 summarizes the crystallinity index values obtained from XRD. Peak 1 corresponds to the I_α 100 and I_β 1̄10 lattice planes, peak 2 to the I_α 010 and I_β 110 planes, and peak 3 to the I_α 110 and I_β 200 planes, respectively.³⁵ It has previously been observed that peaks 1 and 3 shift to wider angles and peak 2 shifts to slightly lower angles upon transition from an I_α -dominated structure to an I_β -dominated structure.³⁵ In the present work, only peaks 1 and 3 were observed to clearly shift in position, while the results are inconclusive regarding the shift of peak 2 due to variation between duplicate samples.

Analysis of d -spacings (d_1 , d_2 , and d_3) and crystallite dimensions (L_1 , L_2 , L_3) was performed from the fitted XRD data as summarized in Table 3. It is seen from this table that the crystallite dimensions were unaltered by the TEMPO-mediated oxidation whereas a tendency to diminished crystallite size was observed following the thermal annealing.

Cotton-ramie type (I_β -dominated) and algal-bacterial type (I_α -dominated) celluloses can be spatially discerned by plotting d_2 versus d_1 , as proposed by Wada and coauthors.³⁵ The same type of observation can be made for the materials in this work as shown in Figure 5. It is clearly seen that the annealed I_β -dominated samples are spatially separated from the I_α -dominated samples.

SEM was used to try to observe any major morphological changes in the highly crystalline cellulose following thermal annealing and TEMPO-mediated oxidation. It has been

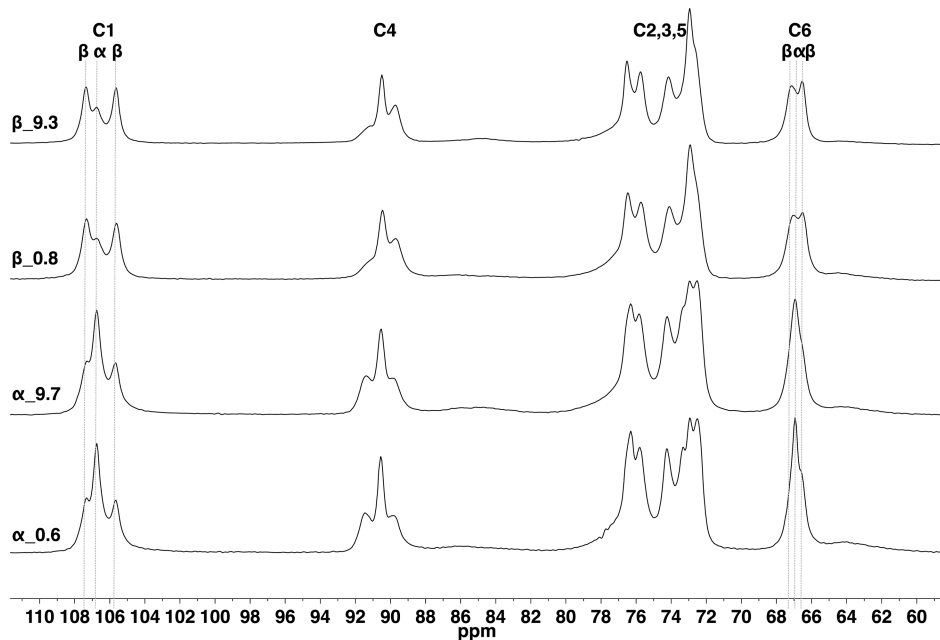


Figure 2. Solid-state CP/MAS ^{13}C NMR full spectra of pristine and annealed *Cladophora* nanocellulose samples $\alpha_0.6$, $\alpha_9.7$, $\beta_0.8$, and $\beta_9.3$. Full spectra for all samples, including samples $\alpha_1.3$ through $\alpha_7.5$, are shown in Supporting Information, Figure S2.

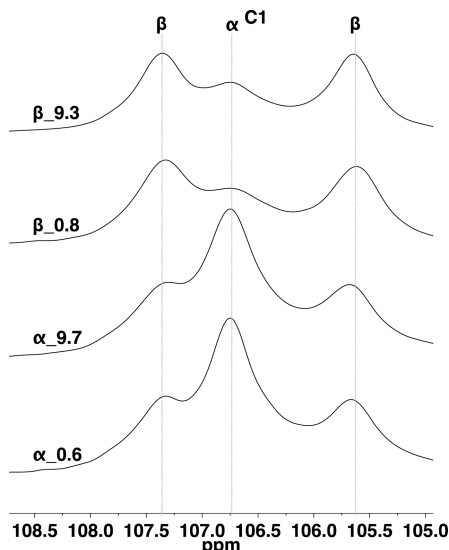


Figure 3. Solid-state CP/MAS ^{13}C NMR spectra for the C1-region of pristine and annealed *Cladophora* nanocellulose samples $\alpha_0.6$, $\alpha_9.7$, $\beta_0.8$, and $\beta_9.3$.

previously observed that following enzymatic degradation I_β -rich fibrils become thinner and defibrillate, whereas I_α -dominated fibrils become shorter.³⁶ Further, AFM analysis has suggested that removal of the I_α fraction not only shortens the fibrils but also increases the surface roughness, resulting in steps and terraces on the fibril surface.³⁶ SEM micrographs for $\alpha_0.6$, $\alpha_9.7$, $\beta_0.8$, and $\beta_9.3$ are shown in Figure 6. No major increase in surface roughness or major shortening of the fibers was observed in this study as a result of oxidation. However, β -dominated samples consist of a higher degree of aggregated fibers than α -dominated samples and this may be a result of the annealing procedure or the fact that different drying procedures were employed for the pristine and the annealed cellulose before oxidation.

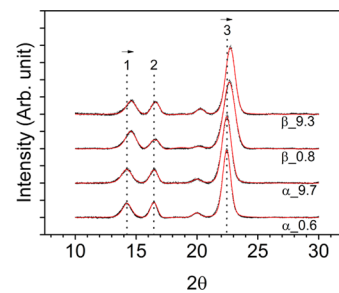


Figure 4. X-ray diffractograms of pristine and annealed *Cladophora* nanocellulose samples $\alpha_0.6$, $\alpha_9.7$, $\beta_0.8$, and $\beta_9.3$. Solid lines correspond to the curve fits made to experimental data (dots) after background reduction. Full diffractograms for all samples, including samples $\alpha_1.3$ through $\alpha_7.5$, are shown in Supporting Information, Figure S3.

It can be concluded that thermal annealing of highly crystalline cellulose from *Cladophora* algae in glycerol resulted in successful transition of I_α -dominated cellulose to I_β -dominated type without substantially affecting its other solid-state properties, such as degree of crystallinity. The successful transition from I_α to I_β -dominated cellulose by thermal annealing was evidenced by three independent methods, that is, FTIR, CP/MAS ^{13}C NMR, and XRD. The subsequent electrochemically controlled TEMPO-mediated oxidation resulted in entire surface carboxylation of cellulose fibril with high degree of oxidation, namely, 9.3–9.7%. This indicates that there is no difference in susceptibility to TEMPO-mediated oxidation between I_α and I_β -dominated cellulose.

Previous experimental evidence suggests that the I_α allotomorph is thermodynamically less stable and therefore more reactive than I_β cellulose.^{10,23} However, it was hitherto unclear if there was a difference in susceptibility to TEMPO-mediated oxidation between I_α - and I_β -dominated cellulose. As was concluded above, there seems to be no difference in susceptibility. The most plausible explanation for this result is that TEMPO-oxidation does not proceed beyond the surface

Table 3. Estimated Values for *d*-Spacings and Crystallite Dimensions^a (*n* = 2)

sample name	d1 (Å)	d2 (Å)	d3 (Å)	L1 (Å)	L2 (Å)	L3 (Å)
$\alpha_{_0.6}$	6.214 ± 0.005	5.375 ± 0.004	3.955 ± 0.002	87.07 ± 2.78	115.30 ± 0.97	99.34 ± 2.478
$\alpha_{_1.3}$	6.236 ± 0.008	5.389 ± 0.001	3.958 ± 0.002	80.17 ± 2.45	109.16 ± 2.30	95.11 ± 3.38
$\alpha_{_2.3}$	6.203 ± 0.013	5.365 ± 0.010	3.948 ± 0.004	82.20 ± 2.52	111.50 ± 0.27	95.81 ± 3.18
$\alpha_{_4.9}$	6.227 ± 0.008	5.383 ± 0.001	3.956 ± 0.002	83.88 ± 1.06	110.86 ± 0.24	97.22 ± 0.52
$\alpha_{_7.5}$	6.192 ± 0.013	5.361 ± 0.013	3.945 ± 0.005	81.75 ± 3.12	104.89 ± 3.24	91.86 ± 4.24
$\alpha_{_9.7}$	6.212 ± 0.007	5.372 ± 0.007	3.949 ± 0.008	78.94 ± 0.28	108.39 ± 2.13	94.78 ± 4.35
$\beta_{_0.8}$	6.098 ± 0.030	5.356 ± 0.018	3.920 ± 0.014	80.01 ± 3.90	101.59 ± 2.01	80.94 ± 6.77
$\beta_{_9.3}$	6.093 ± 0.025	5.356 ± 0.020	3.920 ± 0.015	79.74 ± 4.65	97.46 ± 4.23	80.80 ± 5.94

^aValues represent the mean ± absolute deviation (*n* = 2).

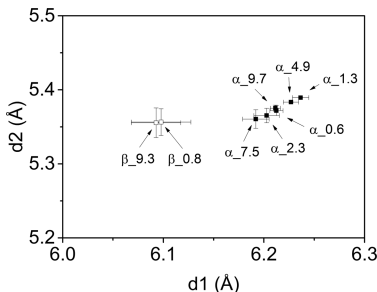


Figure 5. Discriminant *d*-spacing plot for pristine and annealed *Cladophora* nanocellulose samples. The plotted values are the mean ± absolute deviation (*n* = 2).

layer of the crystallites.² Provided that one of the allomorphs is more prone to oxidation than the other and that the oxidation proceeds beyond the surface layer, a gradual increase in the amount of one allomorph paralleled by a decrease in the amount of the other would be expected due to disintegration and dissolution of oxidized chains. Data obtained from three independent methods (XRD, CP/MAS ¹³C NMR, and FTIR) evidenced that no such structural changes occurred. The latter opposes to *Cladophora* cellulose exposed to enzymatic hydrolysis, where I_α -dominated pristine cellulose is transitioned to I_β -dominated structure as a result of preferential hydrolysis of the I_α -fraction.^{9,26}

CONCLUSION

Cladophora cellulose is routinely used as a highly crystalline standard cellulose material featuring high content of the I_α -allomorph. In this study the susceptibility to TEMPO-mediated oxidation of I_α - and I_β -dominated *Cladophora* was explored. The analysis of pristine and annealed TEMPO-oxidized cellulose samples suggests that there is no difference in susceptibility, likely due to the fact that TEMPO-mediated oxidation does not proceed beyond the crystallite surface. This work hence suggests that cellulose from different sources are not expected to differ in susceptibility to the oxidation due to differences in allomorph composition.

ASSOCIATED CONTENT

Supporting Information

Full FTIR, NMR, and XRD spectra, including samples $\alpha_{_1.3}$ through $\alpha_{_7.5}$. This material is available free of charge via the Internet at <http://pubs.acs.org>.

AUTHOR INFORMATION

Corresponding Authors

*E-mail: daniel.carlsson@angstrom.uu.se.

*E-mail: albert.mihryanyan@angstrom.uu.se.

Notes

The authors declare no competing financial interest.

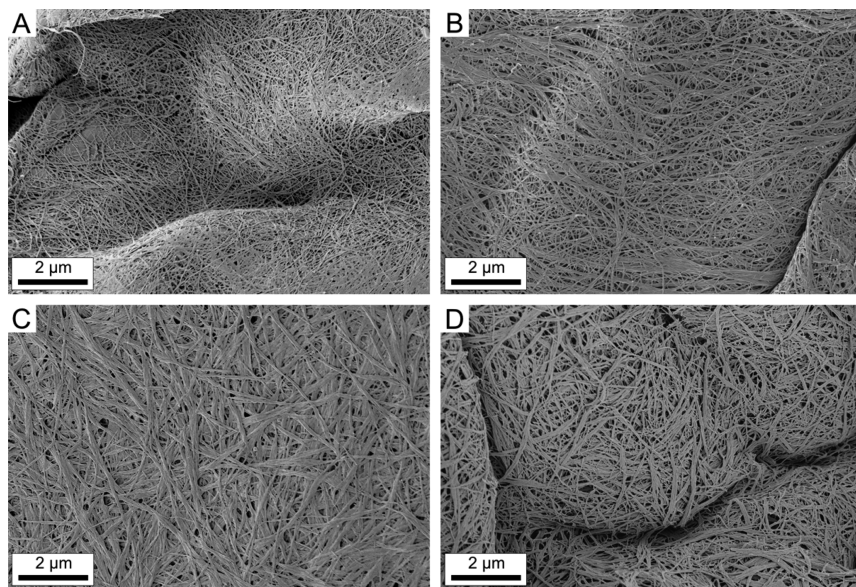


Figure 6. SEM images of pristine and annealed *Cladophora* nanocellulose samples: $\alpha_{_0.6}$ (A), $\alpha_{_9.7}$ (B), $\beta_{_0.8}$ (C), and $\beta_{_9.3}$ (D).

ACKNOWLEDGMENTS

One of the authors (A.M.) is a Wallenberg Academy Fellow and thanks the Knut and Alice Wallenberg Foundation for their support. As well, the Swedish Research Council (VR) and the Swedish Foundation for Strategic Research (SSF) are acknowledged for financially supporting our work. The Swedish NMR Centre is acknowledged for spectrometer time, and Dr. Diana Bernin is acknowledged for sample preparation and for performing the NMR experiments.

REFERENCES

- (1) Milanez, D. H.; do Amaral, R. M.; de Faria, L. I. L.; Gregolin, J. A. *R. Mater. Res.* **2013**, *16*, 635–641.
- (2) Isogai, A.; Saito, T.; Fukuzumi, H. *Nanoscale* **2011**, *3*, 75–81.
- (3) Saito, T.; Hirota, M.; Tamura, N.; Kimura, S.; Fukuzumi, H.; Heux, L.; A. I. *Biomacromolecules* **2009**, *10*, 1992–1996.
- (4) Isogai, T.; Saito, T.; Isogai, A. *Cellulose* **2011**, *18*, 421–431.
- (5) Jin, Y.; Edler, K. J.; Marken, F.; Scott, J. L. *Green Chem.* **2014**, *16*, 3322–3327.
- (6) Carlsson, D. O.; Lindh, J.; Nyholm, L.; Strømme, M.; Mihranyan, A. *RSC Adv.* **2014**, *4*, 52289–52298.
- (7) Okita, Y.; Saito, T.; Isogai, A. *Biomacromolecules* **2010**, *11*, 1696–1700.
- (8) Atalla, R. H.; Vanderhart, D. L. *Science* **1984**, *223*, 283–285.
- (9) Hayashi, N.; Sugiyama, J.; Okano, T.; Ishihara, M. *Carbohydr. Res.* **1998**, *305*, 109–116.
- (10) Atalla, R. H.; Vanderhart, D. L. Cellulose and Wood: Chemistry and Technology. In *Proceedings of the Tenth Cellulose Conference*; Schuerch, C., Ed.; John Wiley and Sons: New York, 1989; pp 169–187.
- (11) Imai, T.; Sugiyama, J.; Itoh, T.; Horii, F. *J. Struct. Biol.* **1999**, *127*, 248–257.
- (12) Belton, P.; Tanner, S.; Cartier, N.; Chanzy, H. *Macromolecules* **1989**, *22*, 1615–1617.
- (13) Jarvis, M. C. *Carbohydr. Res.* **2000**, *325*, 150–154.
- (14) Yamamoto, H.; Horii, F.; Odani, H. *Macromolecules* **1989**, *22*, 4130–4132.
- (15) Sugiyama, J.; Okano, T.; Yamamoto, H.; Horii, F. *Macromolecules* **1990**, *23*, 3196–3198.
- (16) Horii, F.; Yamamoto, H.; Kitamaru, R.; Tanahashi, M.; Higuchi, T. *Macromolecules* **1987**, *20*, 2946–2949.
- (17) Debzi, E.; Chanzy, H.; Sugiyama, J.; Tekely, P.; Excoffier, G. *Macromolecules* **1991**, *24*, 6816–6822.
- (18) Wada, M.; Kondo, T.; Okano, T. *Polym. J.* **2003**, *35*, 155–159.
- (19) Briois, B.; Saito, T.; Pétrier, C.; Putaux, J.-L.; Nishiyama, Y.; Heux, L.; Molina-Boisseau, S. *Cellulose* **2013**, *20*, 597–603.
- (20) Hirai, A.; Horii, F.; Kitamaru, R. *Macromolecules* **1987**, *20*, 1440–1442.
- (21) Yamamoto, H.; Horn, F. *Cellulose* **1994**, *1*, 57–66.
- (22) Uhlén, K. I.; Atalla, R. H.; Thompson, N. S. *Cellulose* **1995**, *2*, 129–144.
- (23) Sassi, J.-F.; Tekely, P.; Chanzy, H. *Cellulose* **2000**, *7*, 119–132.
- (24) Sassi, J.-F.; Chanzy, H. *Cellulose* **1995**, *2*, 111–127.
- (25) Wada, M.; Okano, T. *Cellulose* **2001**, *8*, 183–188.
- (26) Hayashi, N.; Sugiyama, J.; Okano, T.; Ishihara, M. *Carbohydr. Res.* **1998**, *305*, 261–269.
- (27) Horikawa, Y.; Sugiyama, J. *Biomacromolecules* **2009**, *10*, 2235–2239.
- (28) Mihranyan, A. *J. Appl. Polym. Sci.* **2011**, *119*, 2449–2460.
- (29) Debzi, E. M.; Chanzy, H.; Sugiyama, J.; Tekely, P.; Excoffier, G. *Macromolecules* **1991**, *24*, 6816–6822.
- (30) Miller, J. N.; Miller, J. C. *Statistics and Chemometrics for Analytical Chemistry*, 6th ed.; Pearson/Prentice Hall: Harlow, England, 2010.
- (31) Åkerblom, M.; Hinterstoisser, B.; Salmén, L. *Carbohydr. Res.* **2004**, *339*, 569–578.
- (32) Imai, T.; Sugiyama, J. *Macromolecules* **1998**, *31*, 6275–6279.
- (33) Teeäär, R.; Serimaa, R.; Paakkari, T. *Polym. Bull.* **1987**, *17*, 231–237.
- (34) Segal, L.; Creely, J.; Martin, A.; Conrad, C. *Text. Res. J.* **1959**, *29*, 786–794.
- (35) Wada, M.; Okano, T.; Sugiyama, J. *J. Wood Sci.* **2001**, *47*, 124–128.
- (36) Hayashi, N.; Kondo, T.; Ishihara, M. *Carbohydr. Polym.* **2005**, *61*, 191–197.